B. Maker
Graduate Student,
Aerospace Engineering Department.

S. K. Samanta
Professor,
Mechanical Engineering and
Applied Mechanics Department.
Fellow ASME

The University of Michigan,
Ann Arbor, MI 48109-2125

G. Grab
Metallurgy Department,
Research Staff,
Ford Motor Company,
Dearborn, MI 48121-2053

N. Triantafyllidis
Associate Professor,
Aerospace Engineering Department,
The University of Michigan,
Ann Arbor, MI 48109
Mem. ASME

An Analysis of Drawbeads in Sheet Metal Forming: Part II—Experimental Verification

This paper presents experimental results obtained for a variety of drawbeads typical of automotive applications, and compares the results with those obtained from the numerical model presented in the first part of this work (Triantafyllidis et al., 1986). The deformation process is divided into two phases: the "locking/clamping" phase as the binder closes to form the sheet around the drawbead, and the "pulling" phase as the panel is formed, causing the material to be drawn through the bead. Metals considered are SKDQ steel, aluminum, and brass. Dry and lubricated conditions are investigated. Good correlations between model and experiment are obtained for strain distributions over the sheet and excellent agreement is observed in the binder clamping forces. Using a Coulomb friction law in the model, horizontal restraining forces are compared to experimental results. The model is shown to accurately predict the influence of variations in material, geometry, and friction conditions. However, the correlation between the model and experiment is not as good in two cases: as the punch (male bead) reaches the "locked" condition, and in the initial stages of "pulling" deformation. Reasons for the discrepancies are discussed.

1 Introduction

Sheet metal forming operations to produce automotive outer body panels involve a two step process. First the binder clamps the sheet metal around the perimeter of the die cavity to hold it in place, and subsequently the punch and die move together to form the part.

The binder surface has recently been an area of design development. It may be flat or angled to elastically precurve the sheet, thereby modifying the points of initial contact between the sheet and punch. The binder's primary function, however, is to provide a restraining force on the sheet to control flow into the die cavity.

A smooth binder surface provides little restraining force, friction being the only active mechanism to control metal flow during forming. Furthermore, no local control of the restraining force is possible, the only control variable being the total binder hold down force. The addition of drawbeads – a raised bead on one binder surface and a mating groove in the other – to the binder surface allows the restraining force to be substantially increased due to the effects of sheet deformation around the drawbead and the increased frictional forces generated during this deformation. By varying the cross-sectional geometry of the drawbead, the designer may modify the restraining force according to the stamping requirements.

It is the purpose of this work to investigate, both analytically and experimentally, the effects of the drawbead on the sheet. The formulation of the problem and the development of the numerical model has been presented by Triantafyllidis et al. (1986). This paper presents experimental results obtained for a variety of drawbeads typical of automotive applications, and compares the results with those obtained from the numerical model.

Previous experiments relevant to this work have considered beads of circular cross section and deformations which have progressed to the steady state condition (Nine, 1978). This investigation considers three bead geometries currently used in metal stamping operations. The deformation process is divided into two phases: the "locking/clamping" phase as the binder closes to form the sheet around the drawbead, and the "pulling" phase as the panel is formed, causing metal to be drawn through the bead. Strain distributions are measured, and binder clamping forces and drawbead restraining forces are monitored, continuously during both phases of deformation. Materials considered are SKDQ steel, aluminum, and brass. Dry and lubricated conditions are investigated, the lubricant being a soap base type common to automotive applications.

2 Experiment

The experimental apparatus, shown in Fig. 1, was designed to allow independent measurement of clamping and pulling forces and their corresponding displacements. Roller bearings were employed to reduce frictional forces associated with the moveable carriages. All load transmission components

Contributed by the Materials Division for publication in the JOURNAL OF ENGINEERING MATERIALS AND TECHNOLOGY. Manuscript received by the Materials Division, May 5, 1986.

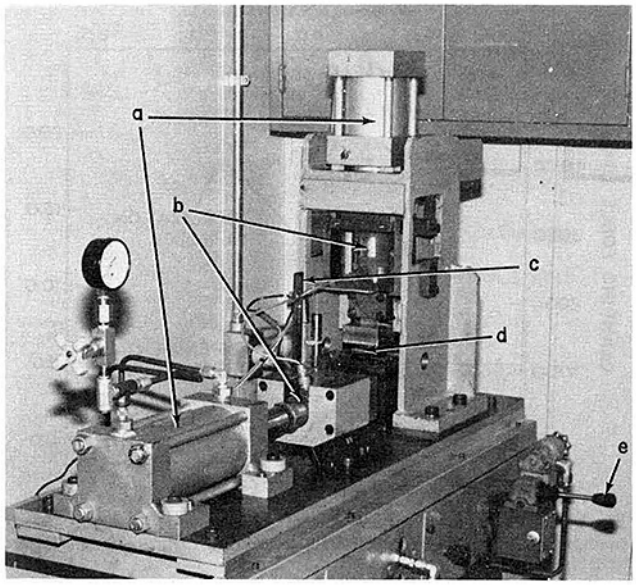

Fig. 1 Experimental apparatus: (*a*) hydraulic cylinders, (*b*) load cells, (*c*) LVDT's, (*d*) test section, and (*e*) control valves

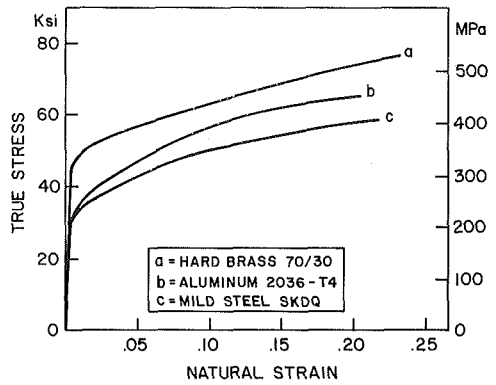

Fig. 2 Tensile test data for (*a*) hardened (as rolled) 70/30 brass, (*b*) 2036-T4 aluminum, (*c*) SKDQ steel

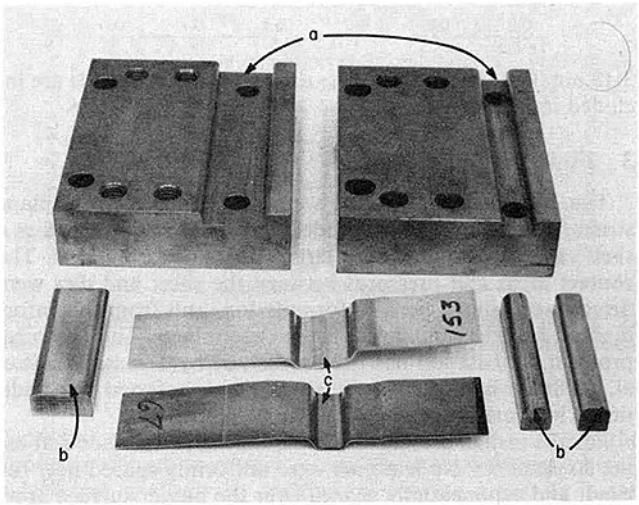

Fig. 3 Various drawbeads and deformed samples: (*a*) female beads, (*b*) male beads, (*c*) aluminum and steel samples

were designed to provide maximum rigidity. A self-contained hydraulic power system was chosen to provide smooth and easily adjustable clamping and drawing velocities.

Equipment. The hydraulic system utilized in the experiment provided up to 6.2 MPa (900 psi.) pressure to two 76.2 mm (3 in.) diameter Sheffer cylinders, one vertical and one horizontal, and was powered by a Lima pumping system. Two Linear Variable Differential Transformers (LVDT's), manufactured by Trans-Tek were used to measure vertical and horizontal displacement. The two load cells used were Lebow Model 3674, each with 44.5 kN (10,000 lb) capacity. A Datronic Model 300D amplifier and a Hewlett-Packard 7004B X-Y recorder were used to measure and record the data.

Samples. Three different materials were used in the experiment, (*a*) SKDQ steel, a common drawing steel, 0.76 mm (0.030 in.) thick, (*b*) 2036-T4 aluminum with a thickness of 1.04 mm (0.041 in.), and (*c*) a 70/30 Brass with a thickness of 0.64 mm (0.025 in.) in the "as rolled" condition. All of the samples were sheared with a standard laboratory hand shear. Standard sample size was 35.6 mm (1.4 in.) wide by 152 mm (6 in.) long. All of the samples used in the experiment were cleaned in an acetone bath to remove protective coatings. Samples were wiped dry with a soft cloth to insure that the surfaces were free of foreign matter. A thin film of Jimini ALQ-1400-A soap based drawing compound was applied to specimens used in lubricated tests. Uniaxial tensile tests were performed on each material, yielding material data for the theoretical model (Fig. 2).

Procedure. For a typical test, a sample was placed onto the moveable carriage and the alignment was checked to insure that its position was perpendicular to the female bead. The sample was clamped into place and then moved hydraulically into position under the male bead and above the female bead. At this point the electronics and LVDT's were balanced and any surge removed from the hydraulic system. Additional clamping devices or stop blocks were added if required. The stop blocks, inserted between the upper and lower binder surfaces near the sample, prevented the male bead from penetrating into the female bead beyond a given depth. For cases presented herein, blocks of 1.1 and 2 sheet thicknesses were used, resulting in separation gaps betweeen the sheet and upper binder of one tenth and one sheet thickness, respectively, at the locked condition.

With all preliminary conditions set, the electronics and recording equipment ready, the male bead was lowered into the female bead, deforming the sample and finally coming to rest on the stop blocks. The electronics were switched from the vertical to the horizontal sensors, and with the male bead held fixed, the carriage was pushed with the horizontal cylinder, pulling the sample through the bead to complete the test. Nominal velocities for punching and pulling were 0.25 mm/s (0.01 in./s). Experimental force-displacement curves presented herein represent an average over at least ten identical tests.

Bead Geometries. Beads were manufactured to specifications similar to those used in automotive applications. Figure 3 shows the actual beads and metal samples which they produce. Three different bead geometries were used in the experiments, hence referred to as "square," "round," and "wide." The square bead has a rectangular cross section typical of automotive beads used with steel; a width of 12.7 mm (0.50 in.), depth of 6.35 mm (0.25 in.), and radii of 3.18 mm (0.125 in.). The round bead is similar except the radii of the male bead are increased to 6.35 mm (0.25 in.), yielding a circular cross section in the male bead. Such a modification is commonly made in industry to allow more material to flow into the die cavity. The wide bead has a geometry typical of beads used in aluminum forming operations, with a width of 25.4 mm (1.0 in.), depth of 6.35 mm (0.25 in.), and radii of

DIMENSIONS (inches) / (mm)

BEAD	b	r	h	B	R	H
ROUND	0.500 / 12.70	0.250 / 6.35	0.250 / 6.35	0.560 / 14.22	0.125 / 3.18	0.310 / 7.87
SQUARE	0.500 / 12.70	0.125 / 3.18	0.187 / 4.75	0.560 / 14.22	0.125 / 3.18	0.310 / 7.87
WIDE	1.000 / 25.40	0.125 / 3.18	0.210 / 5.33	1.100 / 27.94	0.125 / 3.18	0.250 / 6.35

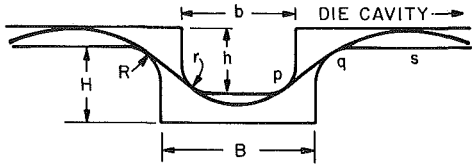

Fig. 4 Drawbead dimensions and sheet position at locked condition (typical). Critical locations on bead are shoulder of male bead (p), shoulder of female bead (q), and binder surface (s)

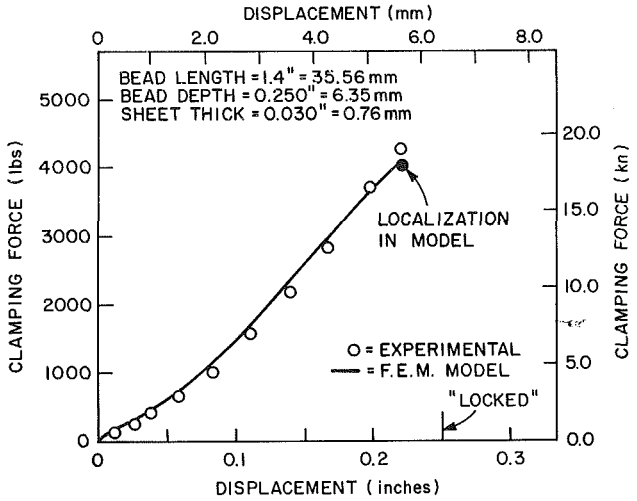

Fig. 5 Clamping force versus vertical displacement for dry SKDQ steel clamped with square bead to locked condition with both ends fixed

3.18 mm (0.125 in.). Complete dimensions of all beads are included in Fig. 4.

3 Finite Element Model

The computer simulations were performed using a plane strain finite element based model. The sheet was modeled as a shell capable of undergoing large strains and rotations. The contact areas and pressures between the sheet and dies were determined using a penalty formulation, and from this information the frictional forces were determined. The complete problem formulation has been presented by Triantafyllidis et al. (1986), where the interested reader is referred for additional information.

For the results presented herein, the sheet was modeled using 80 elements. Node points were uniformly spaced near the bead, and exponentially spaced over the binder surface away from the bead. Element lengths therefore varied from 0.7 sheet thicknesses near the bead to 1.5 thicknesses at the edges of the sheet. Each element contained 15 integration stations in the thickness direction by 4 in the length direction. The foundation stiffness parameter was taken as 50.0, which resulted in penetration depths of the sheet into the foundation always less than one percent of a sheet thickness. The displacement required for the Coulomb friction law to reach 95 percent of its maximum value was 0.02 sheet thicknesses.

Step sizes required for the incremental Newton-Raphson method to converge varied as the simulations progressed. Displacement steps of 0.1–0.5 sheet thicknesses were sufficiently small for most of the simulation. Smaller steps were needed to begin the simulation, as the bead approached the locked condition, and at the onset of the pulling phase of deformation, as strain rates were high during these events. Simulations performed on the University of Michigan Amdahl computer were completed in approximately fifteen minutes of cpu time for each phase of deformation.

4 Results and Observations

Experiments were conducted using two kinds of boundary conditions at the bead. The first set of conditions, denoted "fixed" for simplicity, included clamping devices at each end of the test sheet. During the first stage of deformation, both ends of the sheet were held fixed as the male bead penetrated with the sheet into the female bead. This configuration simulates the conditions experienced by the center bead on a binder surface with three or more beads, the neighboring beads being represented by clamps at some distance from the bead in question. Since motion at each end of the sheet is constrained as the bead is formed, very high mid-surface strains are developed. Numerical experiments using the fixed boundary condition and varied coefficients of friction show that frictional forces have comparatively little effect on the total clamping force and strain distribution. The fixed boundary condition therefore allows experimental verification of the model for the case in which bending, stretching, and contact conditions, rather than frictional ones, govern the process. Experimental verification of this case – where frictional forces are negligible – was a much stronger motivation for this experiment than the relatively rare application where three or more drawbeads are used on the binder surface.

The second boundary condition used, the "free" condition, simulates the actual forming process. The outer edges of the sheet are in reality free to draw into the bead as the binder closes, so a roller boundary condition is used at the edge farthest from the die cavity (left edge), i.e., the sheet was permitted to slide freely but prevented from lifting off the binder surface. Since the entire sheet must remain in place as the binder closes, some points over the die cavity remain fixed as the bead is formed. Hence the right edge of the sample, designated as nearest to the die cavity, was held clamped at some distance away from the bead. In an actual forming operation this distance varies with the size of the die opening, and may be as large as 0.75–1.0 meters (30–40 in.) for some panels. Although the model may readily accept such dimensions, experimental limitations required the sheet be clamped approximately 25 mm (1 in.) from the bead for cases studied herein. This choice of distance causes some small restraining force to be developed at the fixed right edge of the sheet during the first "locking" stage of deformation, but yields force-displacement data at the (ideal) location near the bead. Further experiments were conducted with the sheet clamped at a distance of 150 mm (6 in.) from the bead, eliminating the small initial restraining force, but no appreciable differences were observed in the results.

High Strain Dominated Experiments. Using the fixed boundary condition, dry SKDQ steel and the square bead, clamping force was plotted against penetration depth during the "locking" stage of deformation (Fig. 5). After an initial penetration of approximately one sheet thickness the clamping force increased almost linearly with penetration depth, the slight nonlinearity resulting from the increasing rates of stretching and bending as the bead is formed. The solid line, indicating the numerically calculated clamping force, shows excellent agreement with the experimental data (circles), especially in the initial nonlinear region. A theoretical coeffi-

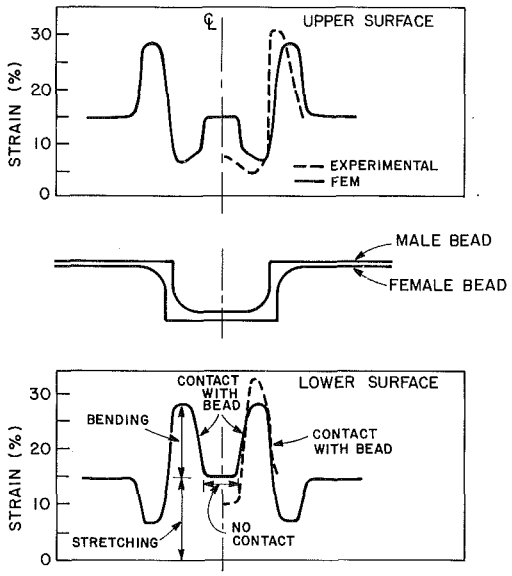

Fig. 6 Experimental and theoretical strain distributions over upper and lower surfaces of dry SKDQ steel sheet locked in square bead with both ends fixed

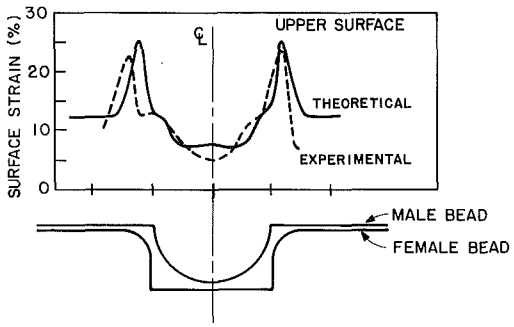

Fig. 7 Experimental and theoretical strain distributions over upper surface of dry SKDQ steel sheet locked in round bead with both ends fixed

cient of friction $\mu = 0.25$ was used in the computation. Localization was predicted by the computation to occur at the end of the solid line, just before the bead locked. Although the actual sheet seemed to survive the anticipated localization point during the clamping phase, initiation of the pulling phase produced immediate necking.

Several samples were photoetched with 0.762 mm (0.030 in.) diameter strain grids. Using the fixed boundary condition, these samples were penetrated to the locked condition, removed from the apparatus, and the strains on the upper and lower surfaces measured. Figure 6 shows the measured (dashed line) and calculated (solid line) strain distribution over the cross section of the square bead after the locking process shown in Fig. 5. Strains are shown on the lower (toward the female bead) and upper (toward the male bead) surfaces of the sheet. Highest strains were measured on the lower surface around the radii of the male bead, and on the upper surface around the shoulders of the female bead – areas where stretching and bending strains were additive. Similarly, lowest strains were measured on the lower surface around the shoulders of the female bead, and on the upper surface around the radii of the male bead. The strain grids were frequently scuffed away in these (contact) areas during the pentration process, yielding incomplete data. The numerical model showed good agreement with the experimental data, both in magnitude and location. In addition the model showed areas of constant strain to be out of contact with the bead, while

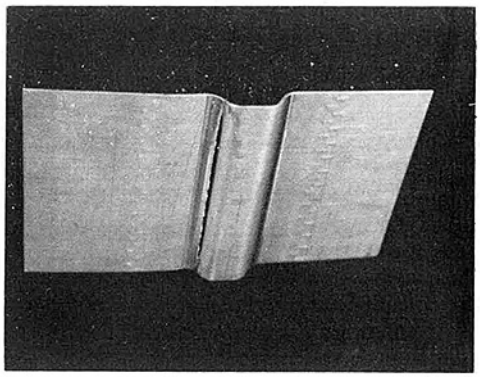

Fig. 8 Photo of localization in dry brass sheet after clamping by square bead to locked condition with both ends fixed

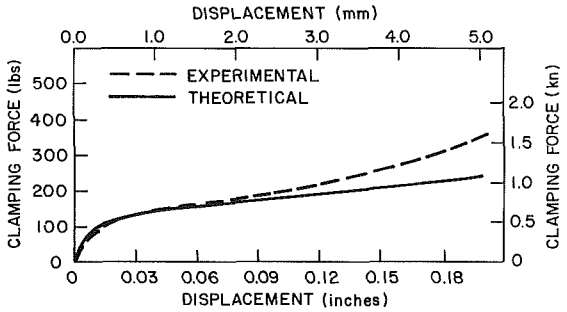

Fig. 9 Clamping force versus vertical displacement curves for lubricated SKDQ steel samples clamped with round bead to locked condition with one end fixed, one end free

areas in contact produced varying strains. As an example, the model predicted no contact across the top of the male bead, which was qualitatively verified by viewing a sample in the locked condition in the test apparatus.

A similar experiment was conducted using the round bead. Since the male half of this bead had a semicircular cross section, contact at the locked position was more uniform, yielding a strain profile on the upper (toward the male bead) surface which was almost nowhere constant (Fig. 7). Strains predicted by the model were again seen to agree well with those obtained experimentally, with the exception of strains near the ends of the sheet. Experimental strains here were lower than those predicted by the model, suggesting less material flowed into the bead than the model anticipated.

The point of localization on the sheet was also identified using the fixed boundary condition. To improve the plane strain condition and delay necking, a 71 mm (2.8 in.) wide sample of hardened (as rolled) brass was used. The penetration process proceeded to the clamped condition using the square bead, followed by the pulling process until failure. Severe stretching and bending combined to produce thinning and subsequent tearing of the sheet, which began at the middle (most nearly plane strain) section and propagated toward the edges. The experiment was halted before the specimen broke completely, and removed for examination (Fig. 8). The localization point, which occurred at the top of the shoulder radius in the female bead, corroborated the position predicted in computation.

Friction Dominated Experiments. Using the free boundary condition, the penetration of the male bead during the locking stage of deformation causes the (free) left edge of the sheet to slide toward the bead, while the right edge is held fixed. The pulling phase of deformation is then implemented by displacing the right edge away from the bead, simulating the main forming operation and eventually causing the entire sheet to bend and unbend as it slips through the bead.

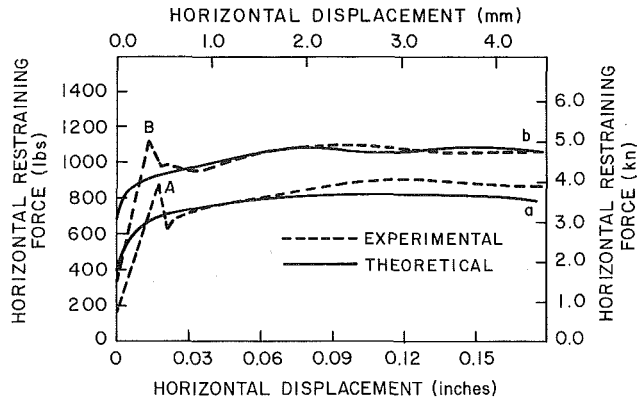

Fig. 10 Variation in lubricant condition. Horizontal restraining force versus horizontal displacement curves for (*a*) lubricated benchmark case, and (*b*) dry SKDQ steel samples penetrated using round bead leaving one tenth sheet thickness separation gap at binder surface.

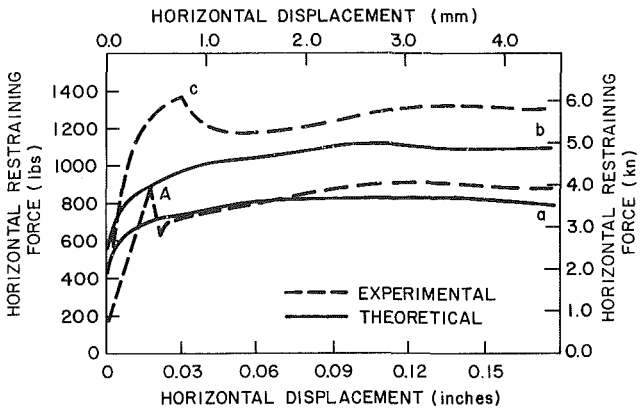

Fig. 11 Variation in bead geometry. Horizontal restraining force versus horizontal displacement curves for lubricated SKDQ steel samples clamped using (*a*) benchmark case round bead, and (*b*) square bead leaving one tenth sheet thickness separation gap at binder surface.

Of foremost importance in these experiments, since they represent the behavior of the bead during an actual forming process, are the horizontal restraining force–horizontal displacement relations for a given set of drawbead conditions. Horizontal forces and displacements reported herein refer to conditions at the edge of the sheet nearest to the die cavity – approximately one inch from the bead. Factors influencing these relations include lubricant condition, bead geometry, separation gap between the sheet and binder surfaces, and material properties. The following results show the effect of independently varying each factor while holding the others constant.

Benchmark Case. As a benchmark case, the round bead is considered when used with a soap based draw compound lubricant and a separation gap of one tenth of a sheet thickness between the sheet and binder surfaces. The punching force-penetration depth relationship (Fig. 9) shows overall forces much lower than those obtained with the fixed boundary condition (shown in Fig. 5) since mid-surface strains were in this case relieved by material flowing from the left (free) edge into the bead. Displacements at the left edge were observed to be approximately 5 mm (0.2 in.). Using a theoretical coefficient of friction $\mu = 0.15$ for the lubricated sheet, experimental and finite element model results show good correlation in the initial stages of clamping. As the bead becomes fully penetrated, however, the experimental punching force increases more rapidly than predicted by the model. This suggests that the sheet actually sticks around the shoulders of the female bead (point q, Fig. 4), rather than flowing into the bead to relieve strains as the computations predict.

After the bead locks against the stop blocks – allowing one tenth of a sheet thickness clearance – the pulling stage of the experiment commences. The clamp holding the right edge of the sheet is used to pull the sheet through the bead, and the restraining force and displacement data are recorded there. Results are given in Fig. 10 (curves {a}) for the pulling stage of the benchmark case, after the clamping process shown in Fig. 9. The initial value of the restraining force is non-zero due to the presence of the clamp during the locking phase, preventing one edge of the sheet from slipping into the bead. The initial value of restraining force predicted by the model is greater than the experimentally observed value, indicating that less material slipped around the shoulder of the female bead (point q, Fig. 4) during locking than expected. Furthermore, the experimental curve increases linearly to a local maximum, then drops sharply, suggesting a stick-slip behavior around the radius of the female bead (point q, Fig. 4). During the experiments the sharp decrease in restraining force was marked by a loud popping noise. The calculated curve shows rather poor agreement throughout this initial range, its gradually decreasing curvature indicating that slippage around the shoulder of the female bead is expected continuously from the onset of pulling. The initial slope of the theoretical curve, taken over the first one tenth of a sheet thickness displacement, does match the initial slope of the experimental curve. At the end of the transient stage, after the sharp decrease in restraining force, the experimental and calculated curves show good correlation as the entire sheet slips through the bead.

Variation in Lubricant. Figure 10 also indicates the effect of variation in lubricant condition. Holding geometry and separation gap constant, the baseline case was varied by omitting the draw compound lubricant (curves {b}). The dry sheet condition produced everywhere larger restraining forces, as expected due to the increase in friction. Behavior differed in the region just after the stick-slip break point. Here the bead with higher friction shows a more gradual reduction in restraining force, unlike the very sharp decline in the lubricated case. This shows that as slippage begins to occur around the shoulder of the female bead, the lubricant acts to further the slipping process, thus causing a more rapid reduction of restraining force in the lubricated case.

Once again, theoretical curves show poor correlation until the entire sheet begins to slip in the bead, after which time the correlation is good. The value of friction coefficient was taken as $\mu = 0.25$ for the dry sheet, and $\mu = 0.15$ for the lubricated sheet. The initial slope of the theoretical curve, taken over the first one tenth of a thickness displacement, does closely match the slope of the experimental curve before slipping occurs.

Variation in Bead Geometry. The effects of variation in bead geometry are illustrated in Fig. 11. Holding lubricant condition and separation gap constant, the benchmark case using the round bead is compared to the case involving the square bead. The geometry of the square bead involves relatively sharp corners in the male bead which concentrate contact area over an even smaller region than in the round bead case. Restraining forces are seen to be everywhere larger for the square bead (curves {b}) than for the round bead (curves {a}). The initial slope of the force-displacement curve for the square bead is linear, but decreases before the break point. This suggests a more complex stick-slip process for the square bead. Material begins to slip over the shoulder of the female bead (point q, Fig. 4), but remains stuck briefly at the radius of the male bead (point p, Fig. 4), where contact pressures are also high. As the displacement continues, the sheet breaks free around the male bead, a popping noise is noticed, and the restraining force falls. Again, the decrease in

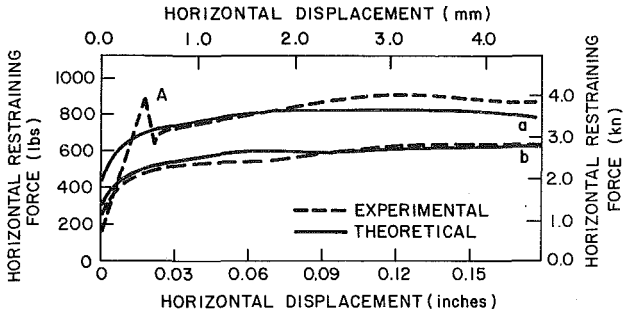

Fig. 12 Variation in separation gap. Horizontal restraining force versus horizontal displacement curves for lubricated SKDQ steel samples clamped using round bead leaving (*a*) benchmark case one tenth, and (*b*) one sheet thickness gap at binder surface.

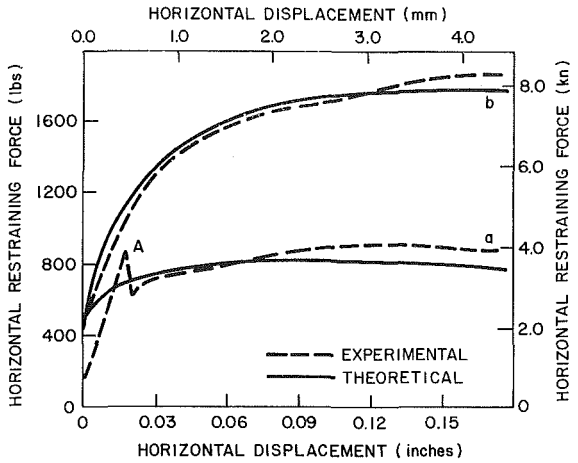

Fig. 13 Variation in material. Horizontal restraining force versus horizontal displacement curves for lubricated condition using aluminum and wide bead leaving one tenth sheet thickness at binder surface.

restraining force is more gradual using the square bead, where sharper radii cause higher contact pressures and increased friction, preventing the sheet from slipping as rapidly as in the benchmark case. The theoretical curve shows consistently lower values of restraining force than the experimental curve, the Coulomb friction model predicting only a portion of the increase in restraining force due to the sharper corners of the square bead.

Variation in Separation Gap. Keeping lubricant and geometry constant, Fig. 12 shows the effect of varying the separation gap between the sheet and binder surface at the locked configuration. The penetration of the male bead during the locking process was halted sooner than in the benchmark case, leaving one sheet thickness clearance between the binder surface and sheet, as compared to one tenth of a thickness for the benchmark case. The sheet did not stick at the shoulder of the female bead during locking in this case, since extreme contact pressures were avoided, resulting in a smoothly increasing force-displacement curve (curves {b}). The linear region at the onset of pulling is no longer present, as material immediately begins slipping over the shoulder of the female bead as the pulling commences. A friction coefficient of $\mu = 0.15$ was assumed in the model of this lubricated experiment. For this case, Coulomb friction provides an adequate model of the process, as evidenced by the excellent correlation in theoretical and experimental data over the entire range of the experiment.

Variation in Material Properties. In the preceding cases it was possible to vary each parameter in turn, while holding the others fixed. Experiments considering aluminum sheets were conducted with the wide bead, a bead of dimensions common to those used in industry for forming aluminum parts. The variation in material properties, therefore, presents a case where bead geometry is necessarily varied as well. Soap based lubricant and a separation gap of one tenth of a sheet thickness are used, consistent with the benchmark case.

Horizontal restraining force is plotted versus horizontal displacement for this case in Fig. 13. The experimental results for aluminum show none of the stick-slip behavior seen in many earlier cases, the initial slope decreasing smoothly from the onset of pulling to the steady state region. Taking a theoretical coefficient of friction $\mu = 0.15$, correlation between theory (solid line) and experiment (dashed line) is exceptionally good, especially in the initial transient stage of the deformation. Experiments with aluminum were also conducted without the draw compound lubricant. In these cases the pulling experiment never reached a steady state condition. Continual stick-slip motion severely damaged the surface of the sheet, leaving large deposits of aluminum on the beads.

5 Discussion and Conclusions

The friction phenomenon involved in drawbead experiments is quite complex. Although the addition of lubricant has a marked effect on the restraining force generated by a particular bead, it is not clear that hydrodynamic pressures are the primary mechanism in reducing friction. Since contact areas are small and usually over the curved shoulders of the bead, lubricant is easily squeezed away from high pressure areas. Coefficients of friction used in the model were chosen to best represent the experimental data as a whole in the steady state region. With coefficeints fixed, computations were performed for variations in geometry, separation gap, and sheet material for both lubricated and dry conditions. These computations determined the coefficients as $\mu = 0.15$ for lubricated cases and $\mu = 0.25$ for dry cases.

Several of the discrepancies between calculated and measured data may be attributed to the inadequacy of the Coulomb friction law adopted in the model to represent the true friction process at very high contact pressures. When relative motion is constrained using the doubly clamped "fixed" boundary condition, the data show excellent correlation even at very large strains (Figs. 5, 6). This demonstrates the accuracy of the contact and finite strain shell theory formulations in the model for a case where numerical experiments have shown frictional effects to be negligible. When relative motion is large, as with the "free" boundary condition, correlation between the model and experiment is poor on two occasions – as the punch reaches the locked condition, and in the initial stages of the pulling deformation – the two cases where contact pressures are maximum. Furthermore, the correlation is not satisfactory for the geometry which has the shapest corners, hence highest contact pressures. Since the accuracy of the contact and strain formulations has been established, these errors may be attributed to the friction portion of the model.

It has been established in the literature (i.e., Dokos, 1946) that for small velocities, extreme contact pressures produce galling and other surface effects which may dramatically increase the effective coefficient of friction. Should this be the case, the local friction coefficient should increase near the shoulders of the drawbeads (points p and q in Fig. 4), causing less slippage around these radii than the Coulomb friction model predicts. This reduced slippage would affect:

- an increase in the calculated punching force as the beads become locked. Axial strains increase in the section of the sheet between the radii of the male and female beads (segment pq in Fig. 4) as they are not relieved by material slipping into the bead.
- a decrease in calculated mid-surface strains in the section of the sheet near the clamp (location s in Fig. 4). Less material flows into the bead during locking.

– a decrease in the calculated initial restraining force. Reduced slippage around the radii during locking prevent strain from being distributed to the clamped end of the sheet.

Each of the above effects of increased friction coefficient in high pressure contact areas would improve the correlation between the model and experiment. Experiments to define how the coefficient of friction should vary with contact pressure for conditions similar to those in drawbeads would be useful. The model could be improved to consider non-Coulomb friction using such data.

In addition to the aforementioned effects, the increase in friction coefficient due to extreme presure would stimulate a stick-slip condition at the initial stages of pulling, as observed experimentally. The slip behavior may not be modeled accurately, however, until the entire dynamic process is considered. Experiments concerning stick-slip friction by a number of authors indicate that the slipping process depends strongly on the dynamic characteristics of the experimental equipment (Bowden and Leben, 1938; Bell and Burdekin, 1969). The additional effort required to consider the fully dynamic problem is outside the scope of this investigation. However, some mention should be made of the importance of stick-slip behavior in the actual stamping operation.

For the cases where contact pressures are not extreme and hence galling, ploughing, and stick-slip friction are avoided, the finite element model has been shown to yield accurate predictions of drawbead behavior. In the cases where extreme contact pressures are achieved, as when the designer desires to completely lock the sheet in place, stick-slip behavior may be observed at the drawbead. If the designer's intention is to completely lock the sheet in place, then any slipping would indicate a bad choice of drawbeads. The designer may be more concerned in this case with the strain distribution across the bead than the restraining force diagram, since this (accurate) information will indicate whether the sheet will tear as the bead is formed.

If the intention is to allow slippage through the bead, the designer may rely on the finite element model to accurately predict the steady state restraining force, and predict an average value of the restraining force generated by the bead during the initial stages of pulling. This averaged behavior may prove to be quite realistic when the entire three dimensional problem is considered. Here the abrupt, dynamic slipping over the bead will be damped by several mechanisms. As the length of the bead is extended to several feet for an actual operation and curved sections are added, neighboring sections will slip at different instants, damping the overall behavior. Similarly, the friction of the sheet on the binder surface will provide local damping during an abrupt slip at the bead. Further experiments using full-scale dies and binders would be useful to examine these effects.

Clearly, the drawbead designer would prefer any slippage through the binder to occur smoothly, as abrupt stick-slip behavior would produce irregularities in the panel. For these cases, the finite element model has the potential to provide an accurate and useful design tool.

Acknowledgments

The authors would like to acknowledge the support of Messrs. J. Heetderks and D. Raffin of Ford Body and Assembly Operations and the financial support from Advanced Engineering and Research funding, Ford Motor Co.

References

Bell, R., and Burdekin, M., 1969–1970, "A Study of the Stick-Slip Motion of Machine Tool Feed Drives," *Proceedings of the Institution of Mechanical Engineers*, Vol. 184, pp. 543–557.

Bowden, F. P., and Leben, L., 1938–1939, "The Nature of Sliding and the Analysis of Friction," *Proceedings of the Royal Society*, Series A, Vol. 169, pp. 371–391.

Dokos, S. J., 1946, "Sliding Friction Under Extreme Pressures," ASME *Journal of Applied Mechanics*, June, pp. 148–156.

Nine, H. D., 1978, "Drawbead Forces in Sheet Metal Forming," *Mechanics of Sheet Metal Forming*, Plenum Press, New York, pp. 203–211.

Triantafyllidis, N., Maker, B., and Samanta, S. K., 1986, "An Analysis of Drawbeads in Sheet Metal Forming Part I – Problem Formulation," ASME JOURNAL OF ENGINEERING MATERIALS AND TECHNOLOGY, Vol. 108, No. 4. Oct., pp. 321–327.